atmosphere

MDPI

Article

Impact of Snow Darkening by Deposition of Light-Absorbing Aerosols on Snow Cover in the Himalayas–Tibetan Plateau and Influence on the Asian Summer Monsoon: A Possible Mechanism for the Blanford Hypothesis

William K. M. Lau [1,*] and Kyu-Myong Kim [2]

[1] Earth System Science Interdisciplinary Center, University of Maryland, College Park, MD 20740, USA
[2] Climate and Radiation Laboratory, NASA/Goddard Space Flight Center, Greenbelt, MD 20771, USA; Kyu-Myong.Kim@nasa.gov
* Correspondence: wkmlau@umd.edu; Tel.: +1-301-405-5395

Received: 21 September 2018; Accepted: 1 November 2018; Published: 12 November 2018

Abstract: The impact of snow darkening by deposition of light-absorbing aerosols (LAAs) on snow cover over the Himalayas–Tibetan Plateau (HTP) and the influence on the Asian summer monsoon were investigated using the NASA Goddard Earth Observing System Model Version 5 (GEOS-5). The authors found that during April–May–June, the deposition of LAAs on snow led to a reduction in surface albedo, initiating a sequence of feedback processes, starting with increased net surface solar radiation, rapid snowmelt in the HTP and warming of the surface and upper troposphere, followed by enhanced low-level southwesterlies and increased dust loading over the Himalayas–Indo-Gangetic Plain. The warming was amplified by increased dust aerosol heating, and subsequently amplified by latent heating from enhanced precipitation over the Himalayan foothills and northern India, via the elevated heat pump (EHP) effect during June–July–August. The reduced snow cover in the HTP anchored the enhanced heating over the Tibetan Plateau and its southern slopes, in conjunction with an enhancement of the Tibetan Anticyclone, and the development of an anomalous Rossby wave train over East Asia, leading to a weakening of the subtropical westerly jet, and northward displacement and intensification of the *Mei-Yu* rain belt. The authors' results suggest that the atmosphere-land heating induced by LAAs, particularly desert dust, plays a fundamental role in physical processes underpinning the snow–monsoon relationship proposed by Blanford more than a century ago.

Keywords: snow darkening; light-absorbing aerosols; dust and black carbon; elevated heat pump effect; snow cover–monsoon relationship; Blanford hypothesis

1. Introduction

Since Blanford [1] first reported a possible inverse relationship, that is, an increased Himalayan snow cover linked to a weakened South Asian summer monsoon (SASM), nearly a century had elapsed before researchers began the rigorous pursuit to better understand the relationship using modern satellite observations and global climate models. Modern studies of the snow–monsoon relationship have provided more diverse perspectives of the original Blanford hypothesis that can be broadly categorized into three overlapping strands. Strand 1 represents work done mostly in the 1970–1990s, in which the original Blanford hypothesis was essentially affirmed, but with additional findings that the relationship might be a component of a broader connection between Eurasian boreal winter and spring snow cover and the South Asian Summer Monsoon (SASM) [2–10]. In Strand 2 (1980 to mid-2000s),

thanks to the advances of modern satellite data, global reanalysis data and global climate models, studies of Eurasian snow cover–monsoon relationships were expanded to include possible impacts on East Asian summer monsoon (EASM) and connections with major modes of global climate variability. Evidence was found that the snow–monsoon relationship could be attributed to the influence of the El Niño Southern Oscillation (ENSO) on both snow cover and monsoon, and that the relationship was strongly masked by the influence of ENSO [11–17]. Included in this strand were also studies showing that the different patterns of Eurasian snow cover were controlled by various modes of natural climate variability, and that during certain periods, increased SASM precipitation was found to be preceded by above-normal winter and spring snow cover over the Tibetan Plateau, contrary to the Blanford hypothesis [18,19]. Others have surmised that a weakening of the snow–monsoon relationship in recent decades may be related to a weakened ENSO–monsoon relationship, possibly due to climate change [20,21].

Strand 3 represents more recent studies from the mid-2000s to the present, where the focus was back on the fundamental physical underpinnings of Blanford's snow–monsoon relationship, by removing or minimizing impacts of remote sea surface temperature (SST) forcing from climate variability. Corti et al. [22] found a strong inverse relationship between Himalayan winter snow cover and Indian monsoon, unless a strong ENSO was present. Wu and Kirtman [23] noted that while ENSO and Tibetan snow cover competed for influence on the Indian monsoon, they cooperated to enhance monsoon precipitation over southern China, via a wave train signal connecting the two regions. Fasullo [24] used a stratified diagnostic methodology and found that in ENSO neutral years, the inverse relationship between the Himalayas–Tibetan Plateau (HTP) snow cover and the Indian monsoon rainfall was highly significant, whereas for Eurasian snow cover the correlation with Indian monsoon rainfall was only modest. Turner and Slingo [25] found similar results in numerical model experiments using the HadCM3 coupled model, indicating that an increase in surface albedo due to more snow cover over the HTP was key to the reduction in surface fluxes leading to a cooling of the Tibetan Plateau, and reduced meridional tropospheric temperature gradient during the early summer, producing therefore a weaker SASM. In related modeling studies, Wang et al. [26] found that a warmer and less snow-covered Tibetan Plateau (TP) could lead to increased summer monsoon precipitation over northern India, and an enhanced subtropical *Mei-Yu* rain belt over East Asia, in conjunction with the development of an upper-troposphere Rossby wave train, spanning the TP and subtropical East Asia. Overall, in all three strands, studies were largely based on observational correlative analyses, which were highly dependent on the spatial and temporal windows chosen. So far, modeling studies to isolate the snow–monsoon relationship have been limited to using various prescribed idealized snow cover changes as boundary forcing to the atmosphere, without consideration of the feedback processes involving snowmelt and atmospheric dynamics. There is a relative dearth of process-oriented modeling studies, especially with regard to the physics of snowmelt. As a result, the fundamental physical processes involved in snow cover change and the interactions with monsoon dynamics remain poorly understood.

Contemporaneous with the Strand 3 studies, there has been an explosive growth in studies of the aerosol–monsoon interactions, indicating that ambient aerosols, both natural and anthropogenic, through direct (radiative) and indirect (microphysical) effects could have a strong impact on Asian monsoon forcing, variability, and change [27–39]. Shielding of solar radiation by aerosols (i.e., solar dimming effect) cools the land surface over Asia, reduces land–sea contrast and thus weakens the monsoon [28]. On the other hand, atmospheric heating by light-absorbing aerosols (LAAs), namely, black carbon (BC), organic carbon (OC) and desert dust, over the Himalayan foothills and Indo-Gangetic Plain can heat the atmosphere, and induce diabatic heating and dynamical feedback via the so-called elevated heat pump (EHP) effect, that could strengthen the early Indian summer monsoon, accelerate the melting of the HTP snowpack, as well as modulate the ENSO influence on the South Asian monsoon [30,32,40–47]. On seasonal and intra-seasonal time scales, the effect of absorbing aerosols may affect the timing and duration of monsoon active and break periods, as well as advance

the monsoon rainy season with increased frequency of extreme precipitation over the Himalayan foothills and northeastern India [48–50].

Another important impact of aerosols on climate stems from the reduction of surface albedo by the deposition of LAAs on snow surface, namely, the snow darkening effect (SDE), causing increased absorption of surface solar radiation and warming of the extratropical land surface and high mountain regions. During the boreal spring, over the snow-covered regions of Eurasia, SDE far exceeds the aerosol dimming effect, resulting in strong positive radiative forcing [51,52]. The efficacy of snowmelt over the HTP, defined as the amount of snow-cover reduction per unit rise in surface warming is much larger due to LAAs than greenhouse warming [53]. Equilibrium climate model experiments show that SDE warms the extratropical Eurasian land surface by up to 2 °C, compared to no-SDE experiments, exerting significant impacts on the water and energy balances and hydro-climate of the Northern Hemisphere continents [54–57]. Based on historical data, significant quantities of LAAs have been found in snowpack and glaciers in the HTP due to local emissions over South Asia, as well as remote transport from afar, causing increases in surface solar radiation absorption via SDE by 5–20 Wm^{-2} [54,58,59]. However, the roles of SDE on HTP snow cover on the Asian summer monsoon and the relevance to the snow–monsoon relationships have not been investigated. The objective of this paper is to shed new light on physical processes involving snowmelt induced by SDE over the HTP, and subsequent interactions with aerosol transport, atmosphere-land heating processes, and monsoon dynamics.

2. Model and Methodology

To obtain the SDE impacts on the Asian summer monsoon (ASM), the authors carried out numerical experiments using the NASA Goddard Earth Observing System Model Version 5 (GEOS-5) climate model [60], under prescribed sea surface temperature (SST) and polar land ice and sea ice conditions. The land surface model in GEOS-5 is the catchment model [61,62], which uses the snowpack model of Lynch-Stieglitz [63]. In this study, the authors used the newly developed GOddard SnoW Impurity Model (GOSWIM) snow darkening physics package which includes radiative transfer calculations of snow albedo and mass distributions of deposited constituent aerosols of dust, BC, and OC in snow [64,65]. Aerosol emission, transport and radiative processes were provided by the Goddard Chemistry Aerosol Radiation and Transport (GOCART) module [66]. The LAAs in GOCART consisted of wind-generated mineral desert dusts [67], prescribed climatological black carbon (BC) and organic carbon (OC) emissions from anthropogenic and natural sources including fossil fuel and biomass burning [68,69]. The version of GEOS-5 used in this study did not include effects of aerosol–cloud microphysics interactions [70].

Two sets of 10-member ensemble experiments were carried out. Each member consisted of a 10-year simulation forced by prescribed observed SST from 2002–2011 [71], but with different atmospheric initial conditions, using the GEOS-5 model at 2° × 2.5° latitude–longitude horizontal resolution and with 72 vertical layers. The first set of experiments (referred to as SDE) employed the fully interactive land surface and snow processes including the GOSWIM SDE physics module. The second set of experiments (referred to as NSDE) was identical to the first except for the absence of SDE physics, that is, constituents are not tracked in the snowpack and do not affect the snow's surface albedo. Atmospheric heating by LAAs were included in both SDE and NSDE. The impacts of SDE on monsoon climate were evaluated based on anomaly fields, defined as the difference in the ensemble mean climatology of the two experiments (SDE–NSDE), each climatology being based on the full 100 years of simulation (10 years × 10 ensemble members). The statistical significance of the results was evaluated using the Student's *t*-test. Further details of the model setup and comparison of ensemble mean climates of SDE and NSDE can be found in two related previous studies based on the same experiments, revealing the importance of SDE on continental scale water and energy balances over the Northern Hemisphere continents [56], as well as on hydro-climate feedback, increasing frequency of heat waves over extratropical Eurasia land, during boreal spring and summer [57]. Model climatologies

of monsoon rainfall, winds, temperature, aerosol optical depth (AOD), and snow cover were validated with data from the Tropical Rainfall Measuring Mission (TRMM), the NASA Modern Era Retrospective Analysis for Research and Application, Version 2 (MERRA-2) reanalysis, and the MODerate-resolution Imaging Spectroradiometer (MODIS), respectively. In this work, the authors focused on the physical mechanisms of SDE impact on snow cover in the Himalayas–Tibetan Plateau (HTP) and the subsequent influence on the ASM.

3. Results

In this section, the authors discuss, in order, (a) the monsoon–snow–aerosol climatology and comparison with observations, (b) the SDE-induced forcing and dynamical feedback processes, (c) the changes in the mean monsoon equilibrium climatic states, and (d) the implication of the authors' results on the fundamental physical underpinning of the Blanford hypothesis. At the outset, it is important to point out that the model LAAs considered here consisted of only primary aerosols (i.e., desert dust, BC, and OC). Chemical processes and secondary aerosol formation were not included. Dust aerosols, as in nature, are treated as intrinsic components of the aerosol–snow–monsoon climate system, with emission rates internally generated as functions of surface winds, atmospheric stability, and soil conditions over deserts and semi-arid regions. On the other hand, model BC and OC emissions are prescribed with seasonal climatology, including both natural and anthropogenic sources. All aerosols are transported by winds and subject to removal by both dry and wet depositions. In this work, the authors focused on the interactions of monsoon dynamics with ambient total aerosols (anthropogenic + natural) on sub-seasonal to seasonal time scales. For brevity, they refer to the sum total of BC and OC as carbonaceous aerosols (CAs) in the following discussion.

3.1. Monsoon–Snow–Aerosol Climatology

To begin, the authors compared the model climatologies of precipitation, winds, aerosol optical depth (AOD), and snow cover over the ASM regions to observations. The model showed overall features representing a reasonably realistic monsoon climate system, with heavy monsoon precipitation over northern India, the Himalayan foothills, and the western Ghats and prevailing low-level southwesterly winds over the region (Figure 1a,e). High AOD over northern India and the Himalayan foothills is due mostly to dust transported from the deserts of the Middle East and West Asia, by the monsoon southwesterlies across the Northern Arabian Sea, and from the Thar deserts to the Himalayan foothills (HF), as well as local emissions from biomass burning and industrial sources over the Indo-Gangetic Plain (Figure 1b,f). Large snow cover fraction is found over the western Himalayas and the southern and northern slopes of the Tibetan Plateau (Figure 1c,g). Compared to observations, the model climatologies had notable discrepancies. Specifically, the model precipitation was excessive over the Himalayan foothills, but too weak, and not as well defined over the eastern Bay of Bengal/western Indo-China regions (Figure 1a,e). These biases were most likely due to the inability of the coarse resolution of the GEOS-5 model to simulate orographic precipitation over complex terrains. Model AODs were too high over the Middle East, and northeastern India and Pakistan (Figure 1b,f). Snow cover was excessive over the western Himalayas and the northern slopes of the TP (Figure 1c,d).

The climatological seasonal cycles of key monsoon control variables show a good match between model and observation (Figure 1d,h). Key features include increasing upper tropospheric meridional temperature gradient and intensifying All-India rainfall (Figure 1d,h, upper panels) during the late boreal spring and early summer monsoon (April–May–June), coincident with a rapid reduction in snow water equivalent (SWE), and increased AOD over northern Arabian Sea and northern India (Figure 1d,h, lower panels). The model AOD peaks in April-May, in advance of the peak in rainfall (July), reflecting the seasonal progression of competing effects of aerosol emission, transport, and precipitation washout, in general agreement with ground-based observations from AERONET [72–74], but slightly in advance of MODIS AOD, which peaks in June–July. Also noteworthy is that the model has maximum

snow cover in March–April–May, compared to January–February–March in the MODIS observations. The reason for the temporal shifts in the model AOD and snow cover compared to MODIS are unclear. Worth noting here is that large uncertainties in snow cover and AOD in the state-of-the-art global climate models and in satellite retrievals still exist. Challenges in comparing model AOD and snow cover to satellite-derived estimates, and the possible impact of model bias in the authors' results, will be discussed in the conclusions (Section 4).

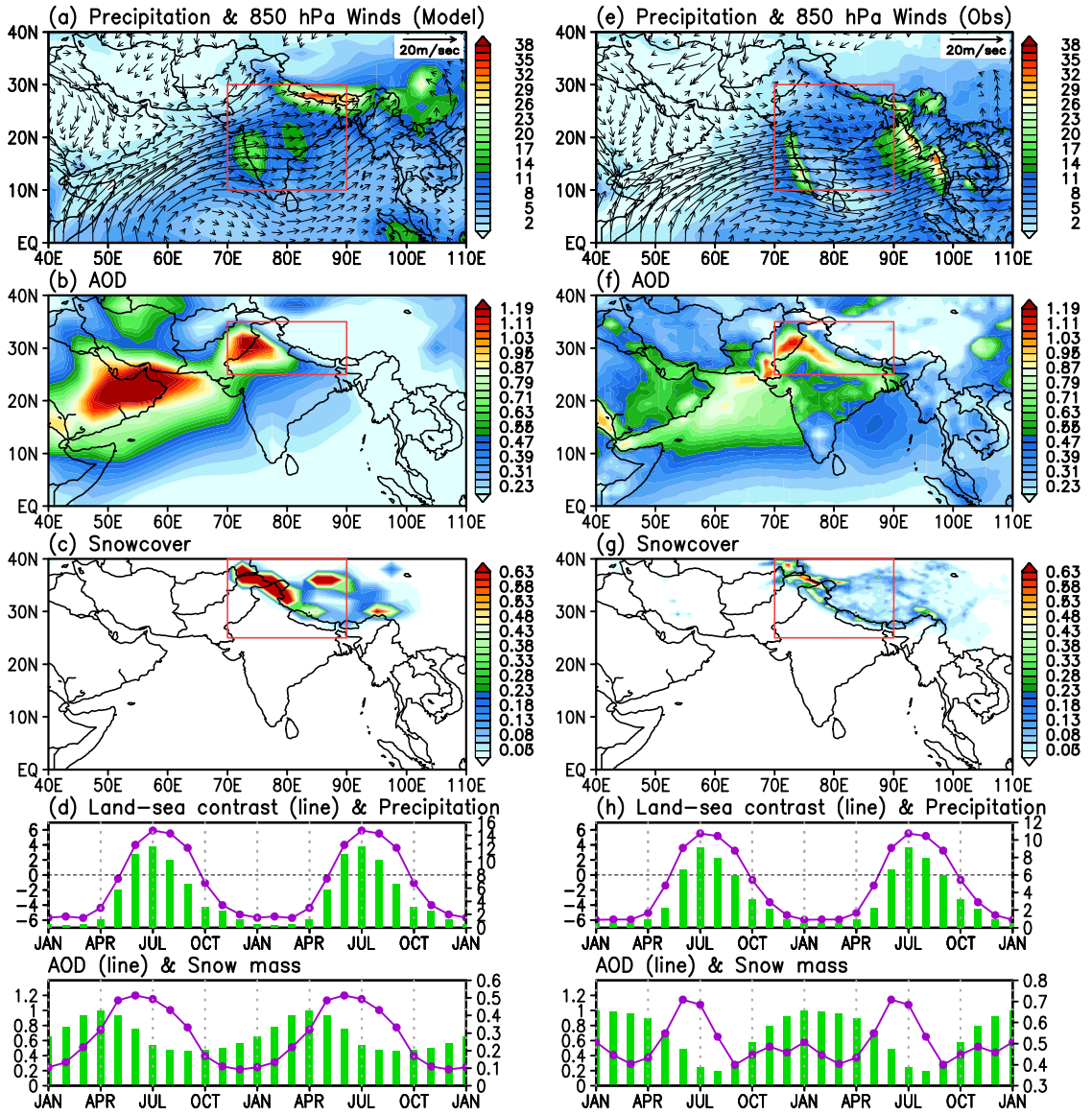

Figure 1. Model June–July–August mean climatology of the control experiment (snow darkening effect (SDE)) for (**a**) precipitation (mm day^{-1}) and 850 hPa winds (m s^{-1}), (**b**) aerosol optical depth (AOD), (**c**) snow cover fraction, and (**d**) seasonal cycle of land–sea contrast (°C), precipitation (mm day^{-1}), AOD, and snow mass, averaged over respective rectangular domains shown in (**a**–**c**), respectively. Land–sea contrast is computed as the temperature difference in the upper troposphere (500–200 hPa), between the northern [70–90° E, 20–30° N] and southern domain [70–90° E, 5° S–5° N]. Panels (**e**–**h**) are the same as (**a**–**d**), except from observations, that is, rainfall (Tropical Rainfall Measuring Mission (TRMM)), winds and temperature (Modern Era Retrospective-analysis for Research and Application, Version 2 (MERRA-2)), AOD, and snow mass (MODerate-resolution Imaging Spectroradiometer (MODIS)) in normalized units.

3.2. SDE-Induced Forcing and Feedback

During the developing phase of the SASM in April–May–June (AMJ), SDE induces a strong reduction in surface albedo (up to 0.3) and increases shortwave (SW) absorption (+5–30 W m^{-2}) over the snow surface, most pronounced along the western, southern, and eastern slopes of the HTP (Figure 2a,b). The increased SW spurs rapid snowmelt and warming of the HTP land surface (Figure 2c,d). Also noteworthy is that in the southeastern and northwestern HTP regions, there are pockets of negative snowmelt flux (Figure 2c), even though the SW surface forcing is positive. This is likely because of enhanced precipitation with enhanced convection and circulation, in the form of increased snowfall at higher elevations of the HTP during AMJ (see the discussion pertaining to Figure 3 in the next subsection), that increases the snow amount (i.e., negative snowmelt flux) over some isolated regions where the rate of snowfall exceeds that of the snowmelt. As the snow cover is reduced, more areas of bare soil are exposed and the warming is accelerated through the snow–albedo feedback [57]. As a result of SDE, the deposition of dust and CA in snow are also increased, especially over the Himalayan foothills (HF), which face the increasing low-level monsoon southwesterlies (Figure 2e,f and Figure 6b later). Note that the large amplitude of the maximum surface warming (>2 °C), and related changes in accelerated snowmelt, loss of snow cover, as well as increased deposition of LAAs in snow, are the result of the full dynamical feedback of the coupled atmosphere–snow–aerosol system, which not only amplifies the initial local SDE warming over the HTP surface, but also exerts influence over extended domains from surface to the upper troposphere spanning the greater ASM regions, lasting through the entire monsoon season, as discussed next.

From May to June, the SDE-induced surface warming ramps up, extending to the upper troposphere over the HTP (Figure 3a,e), by way of increased surface heat fluxes from the warmer land [75,76]. The temperature and wind changes are amplified by increasing shortwave aerosol radiative forcing (ARF) in the atmosphere abutting the HF (Figure 3b,f), as well as by latent heating from increased precipitation over the region (Figure 3d,h). The increased shortwave ARF stems from increased dust accumulation over the HF, as evidenced in their similar distributions indicating increased dust accumulation over the HF (Figure 3c,g). The accumulation of dust in the HF is enhanced by remote transport by the increased low-level southwesterlies from the Middle East deserts, and at the same time, dust is removed by increased precipitation washout. The net increase in dust loading over the HF by SDE indicates that the accumulation outweighs the removal, resulting in a positive net ARF of the atmosphere. In contrast, CAs, which are derived mostly from local emissions, are strongly removed due to SDE-induced increased precipitation washout, providing a negative heating feedback. Since the total ARF is positive in the HF region, the dust heating clearly outweighs any cooling effect due to the removal of CAs. As a result of the aforementioned SDE forcing and feedback, the tropospheric warming peaks in June, in conjunction with the development of a north–south dipole anomaly in zonal winds above 400 hPa over the HTP, and strong anomalous westerlies (easterlies) below (above) 500 hPa over the Indian subcontinent (10–30° N), signaling a strengthening SASM [11,77–80].

The warming of the upper troposphere, associated changes in winds, SW aerosol radiative heating, dust concentration, and precipitation peak in July, over northern India, backing up against the southern slopes of the HTP (Figure 3i–l), and sustained through August (Figure 3m–p). Starting in July, a cooling of the land surface and lower troposphere abutting the Himalayan foothills is noted. This is likely due to the blocking of surface radiation by the increased transport of dust into the region, compounded by increased SW shielding due to increased cloudiness and cooling caused by evaporation of falling rain in an enhanced deep convection [81–83]. Most notable is the fact that while the SDE is letting up due to the climatologically reduced snow cover in the HTP in July-August (see Figure 1d,h), the anomalous shortwave aerosol radiative heating of the atmosphere in the HF remains strong, indicating that atmospheric heating by dust plays a major role in amplifying and strengthening the SASM during July-August. These features are consistent with the EHP mechanism for aerosol–monsoon dynamical feedback, which strengthens the early SASM via atmospheric heating by LAAs [30,34]. Here, the authors found additionally that SDE anchors the action center of the EHP

to the southern HTP and HF where the SDE effect is most pronounced, intensifying the monsoon not only during the early monsoon, but through the entire monsoon season. Note that while these results are robust in the GEOS-5 model, the model has excessive bias in HTP snow cover and AOD, compared to observations. More discussion on how the biases may affect the model results are presented in the conclusions (Section 4).

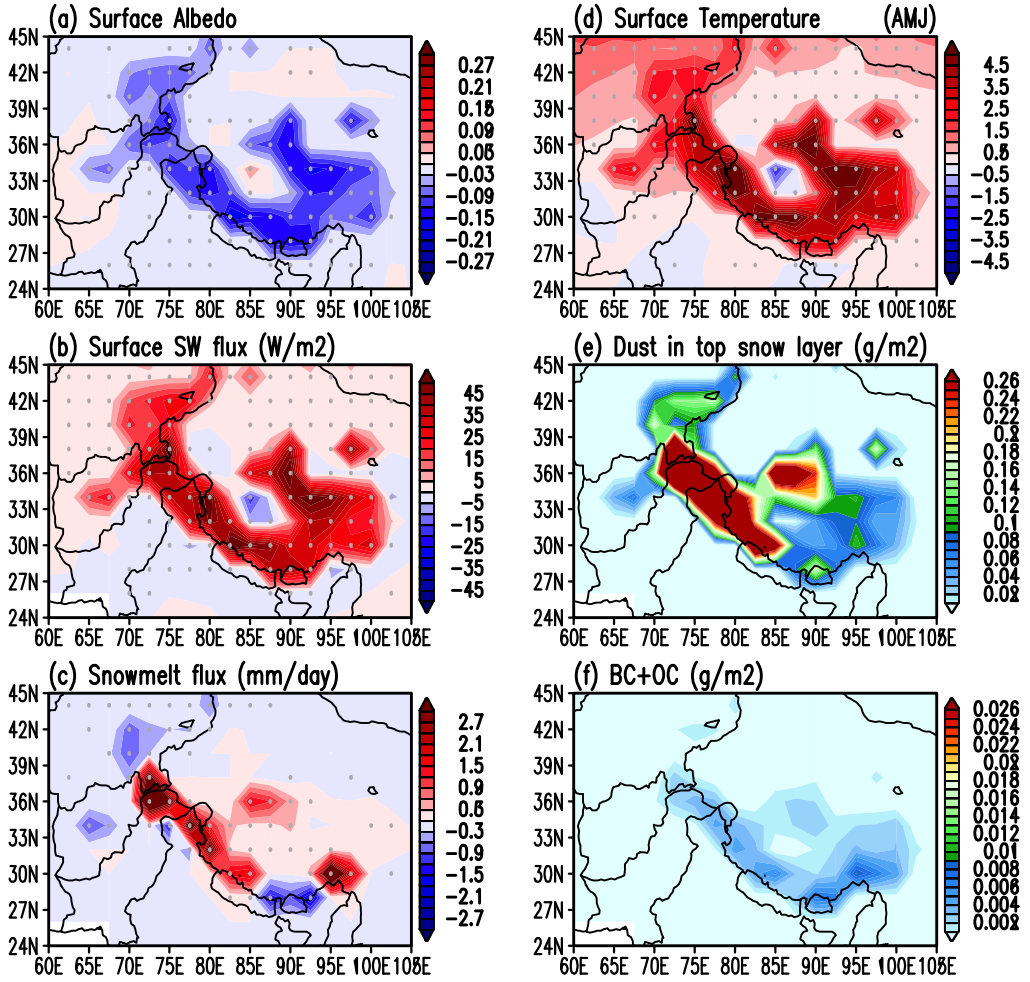

Figure 2. Anomalies induced by snow-darkening effects over the Himalayas–Tibetan Plateau region, for (**a**) surface albedo, (**b**) surface shortwave (SW) fluxes, (**c**) snowmelt, (**d**) surface temperature, (**e**) dust in snow, and (**f**) carbonaceous aerosols (organic carbon (OC) + black carbon (BC)) in snow. Grey dots indicate 95% statistical confidence. Dust and carbonaceous aerosols in snow are set to zero in the second set of experiments (NSDE).

3.3. Changes in Mean Monsoon Climate

As a result of the combined effects of SDE SW forcing and dynamical feedback, the seasonal mean SASM is strengthened as indicated by a well-developed warm anomaly in the upper troposphere over the HTP, sandwiched between a dipole zonal wind anomaly, with increasing easterlies in the tropics 10–30° N, and increasing westerlies in the extratropics 35–50° N (Figure 4a), signaling a strengthening of the Tibetan Anticyclone (TPA) [11,77,79,80]. Another evidence of a strengthened SASM can be found in the increased vertical easterly shear with enhanced low-level westerlies in the lower troposphere below 400 hPa and increased upper level easterlies above at 15° N–30° N [78,84]. In conjunction with the changes in zonal winds and temperature, an enhanced monsoon meridional circulation occurs, featuring increased moistening of the lower and mid-troposphere by anomalous low-level southerlies and deep rising motions over northern India and the HTP. The ascending moister air is coupled to the

anomalous sinking of drier air over southern India and the northern Indian Ocean (0–15° N), and north of the HTP (45–50° N).

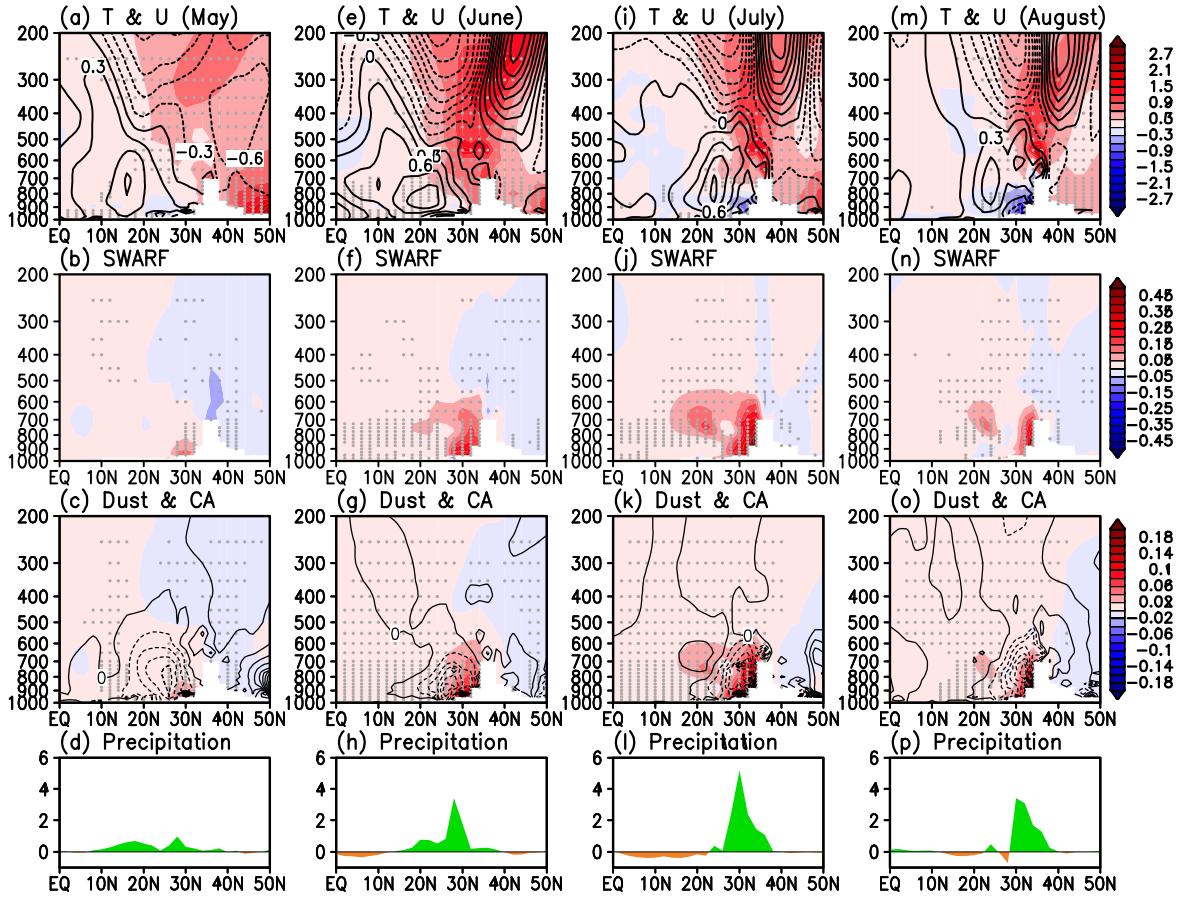

Figure 3. Height–latitude cross-section along 70–90 E, showing anomalies in (**a**) temperature (°C, shaded) and zonal winds (m s^{-1}, contoured), (**b**) atmospheric heating by shortwave radiation (°C day^{-1}), (**c**) concentration of dust (color-shaded in mg Kg^{-1}) and carbonaceous aerosols (CAs) (contoured with negative values dashed, in g Kg^{-1}), and (**d**) precipitation (mm day^{-1}) during May. Panels (**e**–**h**) are the same as (**a**–**d**), except for June. Same for (**i**–**p**), except for July and August, respectively. Grey dots indicate 95% statistical confidence level. SWARF: shortwave aerosol radiative forcing.

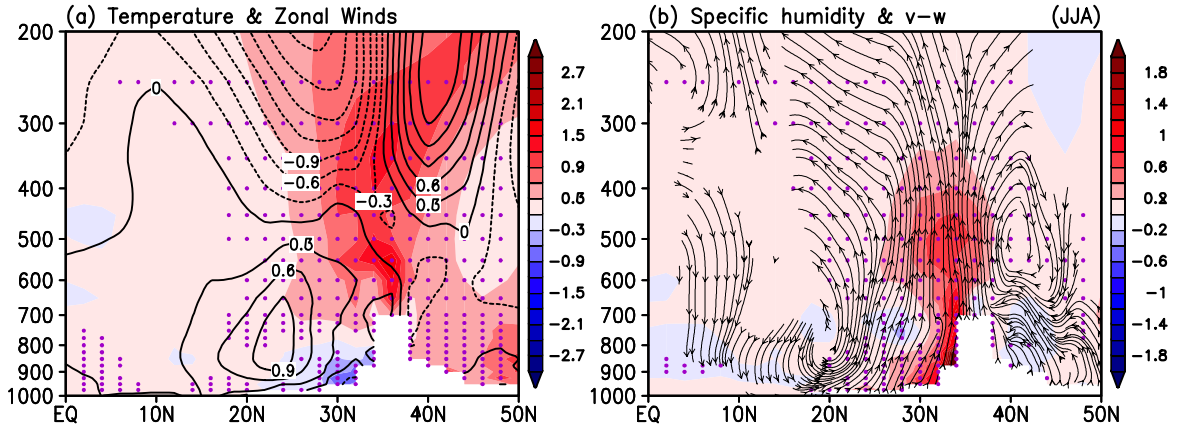

Figure 4. Height–latitude cross-section June–July–August mean anomalies, averaged over (70–90° E) for (**a**) temperature (°C) and zonal winds (m s^{-1}), and (**b**) specific humidity (g Kg^{-1}), and streamlines of anomalous meridional circulation. Purple dots indicate 95% statistical significance.

The SDE in the HTP region impacts not only the SASM, but also the greater ASM regions. The warming of the mid- and upper troposphere arising from the center of action over the high-terrain HTP region (70–90° E) is expansive (Figure 5a), spanning the entire Middle East and Asian monsoon domains (40–120° E). Here, the maximum warming straddles enhanced northerlies (southerlies) to the west (east), consistent with an enhancement of the TPA over the HTP. Emanating from the enhanced TPA is a pattern with alternating meridional winds with opposite signs in the mid- and upper troposphere, spanning a wide range of longitudes (40–130° E). The meridional wind pattern is associated with alternating deep tropospheric rising and sinking motions from the Middle East across South Asia to East Asia (Figure 5b). Increased atmospheric moisture and anomalous rising motions are found most pronounced over the western HTP in northern India/Pakistan (70–90° E) and, to a lesser extent, on the eastern slopes of the HTP and central central-northern East Asia (100–120° E). Further details on the distribution of vertical motions will be discussed with reference to Figure 6 later. Over East Asia, the east–west circulation exhibits a strong westward tilt with height, reflecting the baroclinic tendency of mid- to upper tropospheric extratropical westerlies and interactions with low-level moisture transport, and moisture convergence on the *Mei-Yu* front of the EASM [84–87].

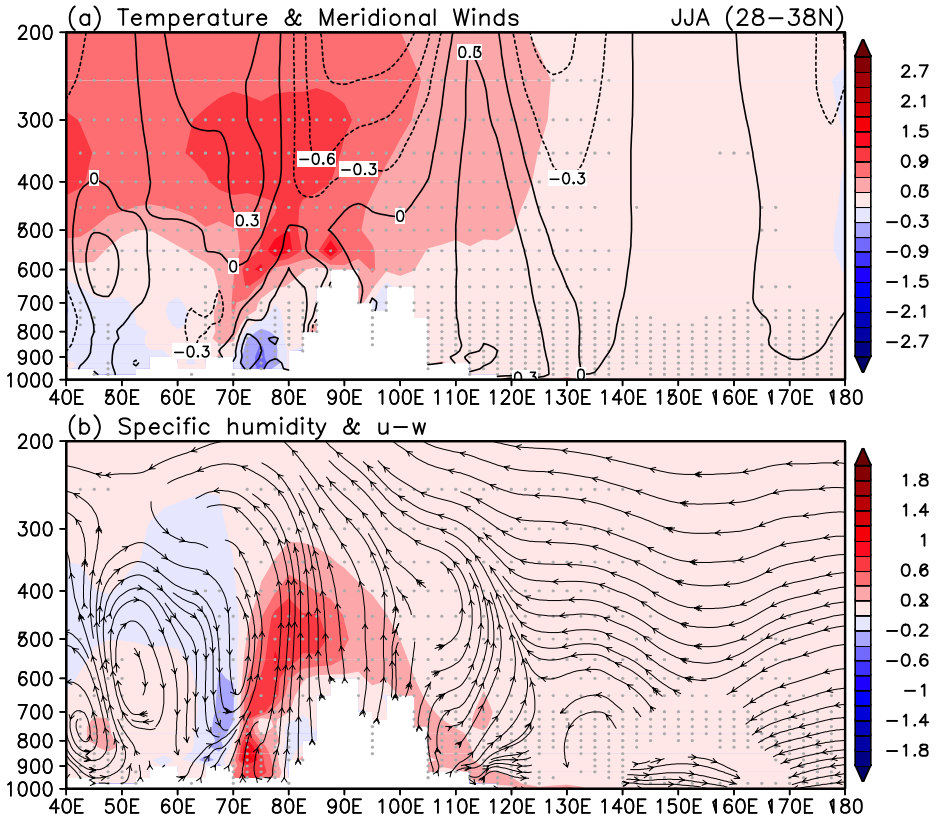

Figure 5. Height–longitude cross-section of June–July–August mean anomalies averaged over (28–38° N) of (**a**) temperature (°C) and meridional winds (m s^{-1}), and (**b**) specific humidity (g Kg^{-1}) and streamlines of anomalous east–west circulation spanning the Middle East to the western Pacific (40° E–180°). Statistically significant values exceeding 95% are indicated by grey dots.

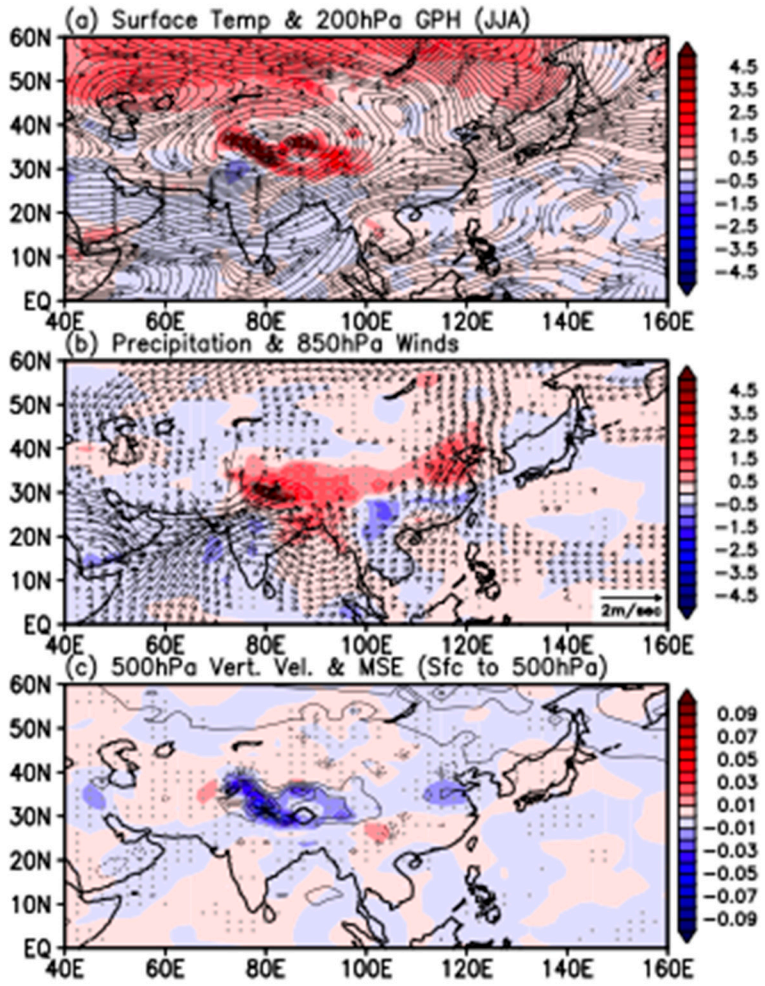

Figure 6. Horizontal distributing showing anomalies in (**a**) surface temperature (°C), and geopotential height at 200 hPa, (**b**) precipitation (mm day^{-1}) and 850 hPa winds (m s^{-1}), and (**c**) vertical motion at 500 hPa (color shading, in units of Pa s^{-1}) and lower troposphere moist static energy (contours, in units of watt m^{-2}). GPH: Geopotential Height.

The aforementioned temperature and circulation features are associated with the formation of an anomalous Rossby wave train, spanning northern Eurasia (30–60° N, 40–140° E), with an enhanced anomalous TPA anchored to the surface heating of the HTP, connected to alternating cyclonic and anticyclonic circulation cells, over northern China/Mongolia, and northeastern East Asia, respectively (Figure 6a). The Rossby wave train occurs in conjunction with an elongated band of anomalous easterlies stretching from the Sea of Okhotsk, across Japan and central China, signaling a weakening of the climatological subtropical East Asian jet (120–160E). The anomalous easterlies continue westward, merging with the southern flank of the enhanced TPA, and further on across the Middle East. The planetary scale nature of the easterly wind anomalies is associated with a warming of the northern Eurasian continent in boreal spring and early summer [56,57], which pre-conditions the snow cover change and warming over the HTP during June–July–August (Figure 6a). As a result of SDE-induced warming over the HTP, the rainfall and circulation patterns of the entire ASM are substantially altered. Increased low-level westerlies transport more dust aerosols from the desert regions across the North Arabian Sea into India, accumulating them over the HF, enhancing the SASM through the EHP positive feedback mechanism. As a result of increased moisture transport by the southwesterlies, precipitation is strongly enhanced over the HTP and northeastern India. The latent heat release from increased precipitation further enhances the warming of atmosphere over the HTP. Over East Asia, precipitation is increased over northern and northeastern China due to the increased

southerly moisture transport from the south, from Indo-China and the South China Sea. For both the SASM and the EASM, a dipole anomalous precipitation pattern (north-positive and south-negative) is found, signaling an intensification, and northward displacement of the climatological monsoon rain belt. Over East Asia, this displacement may signal the "abrupt northward jump" of the *Mei-Yu* rain belt from central to northern China [85–87]. The main driver of the increased rainfall stems from the increased low-level moist static energy (MSE), with a pronounced primary action center over the southern slopes of the HTP, and a secondary center over northeastern China (Figure 6c). These centers feature strong anomalous mid-tropospheric ascent, due to increased latent heating, and orographic uplifting on wind-facing steep slopes of the HF regions (Figure 6c), as well as strong low-level transport of moisture from the Arabian Sea, and from Southeast Asia/South China Sea, respectively. Because of the stable air near the tropopause, the increased ascent over the HTP leads to the shrinking of the air column above, and the development of the anomalous anticyclonic center, enhancing the TPA [26,76].

3.4. A Possible Mechanism for the Blanford Hypothesis

The physical processes underlying changes in the seasonal cycles of key elements of the aerosol–snow–monsoon climate system induced by SDE over the HTP for the SASM are summarized in the context of the Blanford hypothesis (Figure 7). During April–May–June, increased snowmelt and reduction in snow cover over HTP are induced by the deposition of LAAs on the snow cover surface.

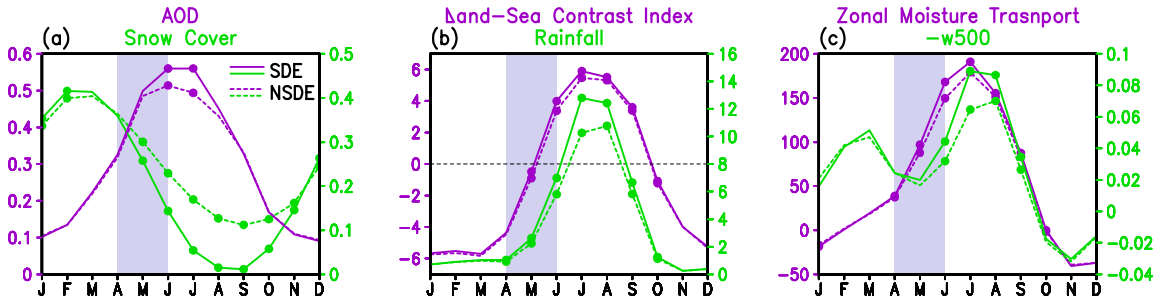

Figure 7. Time series depicting the seasonal cycles of (**a**) snow cover (percentage) and AOD, (**b**) land–sea contrast (°C) and rainfall (mm day^{-1}) over northern India (70–90° E, 25–35° N), and (**c**) westerly low-level (1000–850 hPa) moisture flux (Kg m^{-1} s^{-1}) averaged over the eastern Arabian Sea (70–75° E, 10–30° N) and negative p-velocity (Pa s^{-1}) over northern India. Domains for snow cover and AOD are the same as used in Figure 1. Labels and ordinate units are color-matched to the line plot.

The impurities in snow reduce surface albedo and enhance the absorption of insolation, leading to rapid snowmelt, loss of snow cover, and warming of the land surface and the atmosphere over the HTP (Figure 7b). As the monsoon season advances in May–June, the warming over the HTP is amplified by aerosol–radiation–circulation–precipitation feedback, rapidly extending throughout the upper troposphere over the HTP, increasing the meridional temperature gradient between the monsoon and oceanic regions to the south (Figure 7b), resulting in increased precipitation over northern India in the early monsoon season [25,88,89]. The increased southwesterlies associated with the strengthened early monsoon enhance the dust loading and atmospheric heating over the Himalayan foothills region in northern India, sustaining the feedback through the aerosol "elevated heat pump" mechanism [30,31] through July-August, even when the climatological snow cover over the HTP is significantly reduced (Figure 7a). As a result of the SDE-induced dynamical feedback, the monsoon rainy season is advanced, and the monsoon precipitation over the northern India/HTP region is strongly enhanced in July-August (Figure 7b). Correspondingly, the moisture flux from the East Arabian Sea into the India subcontinent increases in AMJ, peaking in July, while the ascending motion at 500 hPa over the northern India/HTP region is substantially enhanced in June–July–August (Figure 7c), in parallel with the precipitation increase there (Figure 7b). Interestingly, the climatological vertical motion over the region shows a steady increase from November to March and then a decline

in March to May (Figure 7c). A close examination of the seasonal variation of the winds indicates that the vertical motion over this region stems, in part, from orographic forcing of the mid- to upper-level westerlies by the TP, which are strongest in boreal winter. As the monsoon season approaches, the upper westerlies migrate poleward to the north of the TP, and the vertical motion weakens. For this climatological feature, there is little or no difference between SDE and NSDE from November through April (Figure 7c). However, starting in May, as the TP heats up, ascent over northern India/HTP and moisture transport by the low-level monsoon southwesterlies are much stronger in SDE than in NSDE. Indeed, all aforementioned key monsoon indicators signal a strengthening SASM from May through August, due to the SDE-induced reduction in snow cover, but with minimal or no impacts over these regions during the rest of the year. Given the time-lagged relationship between snow cover and increased monsoon rainfall, it is possible that such a relationship could have potential value for predicting the strength of the SASM, as first proposed by Blanford more than a century ago. Based on these relationships, it can be argued that monitoring dust conditions over the Arabian Sea and Northern India during the pre-monsoon season (April to mid-June) could provide value-added information for seasonal-to-interannual predictability of the SASM.

4. Conclusions

Based on numerical simulations using the NASA GEOS-5 climate model, the authors examined the possible impact of snow-darkening effects (SDE) by deposition of light-absorbing aerosols (LAAs) on snow cover over the Himalayas–Tibetan Plateau (HTP), and the subsequent influence on the Asian summer monsoon. Results showed that during April–May–June, LAA deposition on snow reduced surface albedo, increased absorption of surface shortwave radiation, reduced snow cover by rapid snowmelt, and induced a strong surface warming (>2 °C) in the western, southern, and eastern flanks of the HTP. The surface warming extended from the HTP surface to 200 hPa and above, through dynamical feedback processes, associated with an enhanced Asian monsoon, featuring a stronger Tibetan Plateau Anticyclone (TPA), with increased low-level southwesterly flow and increased precipitation over northern India. Increased dust aerosols were transported from the Middle East and from the West Asia and Thar deserts by the strengthened monsoon southwesterlies to the Himalayan foothills (HF) and the Indo-Gangetic Plain (IGP) of northern India. The increased dust transport from remote sources overpowered the wet removal of dust by increased precipitation, resulting in a net increase in dust loading over the IGP. On the other hand, carbonaceous aerosols, which are derived mostly from local sources in the IGP and HF, were strongly removed by increased precipitation washout. The net accumulation of dust aerosols in the IGP and HF plays an important role in heating the atmosphere by shortwave radiative forcing, which is reinforced and sustained by increased latent heating from enhanced precipitation over northern India through July-August, via the elevated heat pump (EHP) mechanism [30,31].

The SDE-induced dynamical feedback leads to a new equilibrium monsoon climate. During June–July–August, the strong warming over the HTP produces an upper tropospheric wave train, with alternating cyclonic and anticyclonic circulation cells that span eastern Europe and East Asia. Anomalous circulation cells, which develop along the wave train, are responsible for a weakening of the East Asian jet and the enhancement of the TPA, that is coupled to increased poleward transport of moisture that spurs a northward shift, and the intensification of precipitation over India and East Asia. The authors found that the SDE-induced rapid snowmelt and warming over the HTP can effectively anchor the EHP dynamical feedback, via strong build-up of moist static energy, anomalous ascent and latent heating in the southern slopes of the HTP, where orographic forcing by the steep topography can provide efficient penetrative convection that transports heat, moisture and aerosols to the upper troposphere and lower stratosphere [90].

As a caveat, the authors note that simulations of monsoon mean states of meteorology, snow cover, and aerosol and the comparison with observations made by state-of-the-art climate models, including the GEOS-5 model used in this study, are still challenging, due to inadequate model

physics, as well as large uncertainties in aerosol and snow products from satellite retrievals [91–94]. In this study, for computation economy of the long-term (100 years) simulation, the authors used a low-resolution version of the GEOS-5 model and emphasized the large-scale interactions. While the model possesses a reasonable monsoon climate, it has non-negligible discrepancies when compared with observations, in that the AOD is too high, snow cover is too much, and rainfall is overestimated over the HF and underestimated in the eastern Bay of Bengal. The GEOS-5 model used here is also known to have a cold bias over continents [56,57], due to the excessive snow cover in Eurasia and the HTP. In the real world, the SDE direct (radiative) forcing is time- and space-limited. Once the ground snow is all melted, the SDE shortwave radiative forcing vanishes, even though the induced anomalies may continue to be amplified by dynamical feedback. In the model, the excessive snow cover means that SDE continues to have an effect even during the peak monsoon season. Hence, the excessive model AOD and snow cover in boreal spring through summer may mean an overestimation of the SDE effects on monsoon compared to the real world, especially when other control factors such as anomalous sea surface temperature forcing are in play.

Nonetheless, from the idealized experiments, the authors' results have shed new light on a possible physical mechanism that underpins the Blanford hypothesis, namely, increased (decreased) deposition of LAAs on HTP snow surface can lead to a decrease (increase) in surface albedo resulting in less (more) snow cover, warming (cooling) of the HTP land and atmosphere, enhanced (reduced) westerly transport of desert dust from the Middle East desert across the North Arabian Sea, and increased (decreased) dust loading and heating of the atmosphere over the HF and the IGP in April–May–June, foreshadowing a robust increase (decrease) in rainfall over northern India in July-August. Given the availability of much improved and reliable multiple data sources from in situ, satellite and reanalysis, specific information on snow cover and aerosols could be systematically diagnosed and incorporated into empirical and model monsoon forecasts, as first envisioned by Blanford (snow cover only) over a century ago. Snow cover and related conditions (temperature, soil wetness, and others) over Eurasia in spring and early summer could also be implemented to improve monsoon seasonal-to-interannual forecasts.

Finally, the results of this study support the new paradigm that LAAs such as desert dust and BC and OC from biomass burning, which are abundant in monsoon regions from natural sources, are intrinsic components of a monsoon climate system, contributing significantly to the distribution heat sources and sinks of the monsoon on multiple time scales [41,95]. A better understanding of the interaction between monsoon dynamics and ambient aerosols (natural and anthropogenic) is essential in further unraveling the causes, consequences, and predictability of climate variability and change in monsoon regions.

Author Contributions: W.K.M.L. conceived the idea of the effect of snow impurity on snow–monsoon interaction, directed the research, and wrote the paper. K.-M.K. contributed to the evaluation of the model experiments and conducted the analysis.

Funding: This research was jointly supported by the Modeling, Analysis, and Prediction Program, National Aeronautics and Space Administration, Grant #5260472 to the University of Maryland, Water Cycle and Extremes Modeling Project, Department of Energy/Pacific Northwest National Laboratory, Grant #4313621 to the University of Maryland. K.M.K. was also partially supported by the NASA High Mountain Asia (HMA) Project.

Acknowledgments: Results of work were based on ensemble experiments conducted using the GEOS-5 model, in collaboration with T. Yasunari and R. Koster, which laid the ground work for this study.

Conflicts of Interest: The authors declare no conflict of interest. The funding sponsors had no role in the design of the study; in the collection, analyses, or interpretation of data; in the writing of the manuscript; and in the decision to publish the results.

References

1. Blanford, H.F. On the connexion of Hamalaya snowfall with dry winds and seasons of drought in India. *Proc. R. Soc. Lond.* **1884**, *37*, 3–22. [CrossRef]

2. Hahn, D.G.; Shukla, J. An Apparent Relationship between Eurasian Snow Cover and Indian Monsoon Rainfall. *J. Atmos. Sci.* **1976**, *33*, 2461–2462. [CrossRef]
3. Dey, B.; Kumar, O.S.B. An Apparent Relationship between Eurasian Spring Snow Cover and the Advance Period of the Indian Summer Monsoon. *J. Appl. Meteorol.* **1982**, *21*, 1929–1932. [CrossRef]
4. Dickson, R.R. Eurasian Snow Cover versus Indian Monsoon Rainfall—An Extension of the Hahn-Shukla Results. *J. Clim. Appl. Meteorol.* **1984**, *23*, 171–173. [CrossRef]
5. Barnett, T.P.; Dümenil, L.; Schlese, U.; Roeckner, E.; Latif, M. The Effect of Eurasian Snow Cover on Regional and Global Climate Variations. *J. Atmos. Sci.* **1989**, *46*, 661–686. [CrossRef]
6. Parthasarathy, B.; Yang, S. Relationships between regional Indian summer monsoon rainfall and Eurasian snow cover. *Adv. Atmos. Sci.* **1995**, *12*, 143–150. [CrossRef]
7. Vernekar, A.D.; Zhou, J.; Shukla, J. The Effect of Eurasian Snow Cover on the Indian Monsoon. *J. Clim.* **1995**, *8*, 248–266. [CrossRef]
8. Sankar-Rao, M.; Lau, K.-M.; Yang, S. On the Relationship between Eurasian Snow Cover and the Asian Summer Monsoon. *Int. J. Climatol.* **1996**, *16*, 605–616. [CrossRef]
9. Dong, B.; Valdes, P.J. Modelling the Asian summer monsoon rainfall and Eurasian winter/spring snow mass. *Q. J. R. Meteorol. Soc.* **1998**, *124*, 2567–2596. [CrossRef]
10. Bamzai, A.S.; Shukla, J. Relation between Eurasian Snow Cover, Snow Depth, and the Indian Summer Monsoon: An Observational Study. *J. Clim.* **1999**, *12*, 3117–3132. [CrossRef]
11. Lau, K.M.; Li, M.T. The Monsoon of East Asia and its Global Associations—A Survey. *Bull. Am. Meteorol. Soc.* **1984**, *65*, 114–125. [CrossRef]
12. Yang, S.; Xu, L. Linkage between Eurasian winter snow cover and regional Chinese summer rainfall. *Int. J. Climatol.* **1994**, *14*, 739–750. [CrossRef]
13. Douville, H.; Royer, J.F. Sensitivity of the Asian summer monsoon to an anomalous Eurasian snow cover within the Météo-France GCM. *Clim. Dyn.* **1996**, *12*, 449–466. [CrossRef]
14. Yang, S. ENSO–snow–monsoon associations and seasonal–interannual predictions. *Int. J. Climatol.* **1996**, *16*, 125–134. [CrossRef]
15. Ferranti, L.; Molteni, F. Ensemble simulations of Eurasian snow-depth anomalies and their influence on the summer Asian monsoon. *Q. J. R. Meteorol. Soc.* **1999**, *125*, 2597–2610. [CrossRef]
16. Liu, X.; Yanai, M. Influence of Eurasian spring snow cover on Asian summer rainfall. *Int. J. Climatol.* **2002**, *22*, 1075–1089. [CrossRef]
17. Zhang, Y.; Li, T.; Wang, B. Decadal Change of the Spring Snow Depth over the Tibetan Plateau: The Associated Circulation and Influence on the East Asian Summer Monsoon. *J. Clim.* **2004**, *17*, 2780–2793. [CrossRef]
18. Robock, A.; Mu, M.; Vinnikov, K.; Robinson, D. Land surface conditions over Eurasia and Indian summer monsoon rainfall. *J. Geophys. Res.* **2003**, *108*, 4131. [CrossRef]
19. Wu, B.; Yang, K.; Zhang, R. Eurasian snow cover variability and its association with summer rainfall in China. *Adv. Atmos. Sci.* **2009**, *26*, 31–44. [CrossRef]
20. Kumar, K.K.; Balaji Rajagopalan, B.; Cane, M.A. On the weakening relationship between the Indian monsoon and ENSO. *Science* **1999**, *284*, 2156–2159. [CrossRef] [PubMed]
21. Kripalani, R.; Kulkarni, A.; Sabade, S. Western Himalayan snow cover and Indian monsoon rainfall: A re-examination with INSAT and NCEP/NCAR data. *Theor. Appl. Climatol.* **2003**, *74*, 1–18. [CrossRef]
22. Corti, S.; Molteni, F.; Branković, Č. Predictability of snow-depth anomalies over Eurasia and associated circulation patterns. *Q. J. R. Meteorol. Soc.* **2000**, *126*, 241–262. [CrossRef]
23. Wu, R.; Kirtman, B.P. Observed Relationship of Spring and Summer East Asian Rainfall with Winter and Spring Eurasian Snow. *J. Clim.* **2007**, *20*, 1285–1304. [CrossRef]
24. Fasullo, J. A Stratified Diagnosis of the Indian Monsoon—Eurasian Snow Cover Relationship. *J. Clim.* **2004**, *17*, 1110–1122. [CrossRef]
25. Turner, A.G.; Slingo, J.M. Using idealized snow forcing to test teleconnections with the Indian summer monsoon in the Hadley Centre GCM. *Clim. Dyn.* **2011**, *36*, 1717–1735. [CrossRef]
26. Wang, B.; Bao, Q.; Hoskins, B.; Wu, G.; Liu, Y. Tibetan Plateau warming and precipitation changes in East Asia. *Geophys. Res. Lett.* **2008**, *35*, L14702. [CrossRef]
27. Babu, S.S.; Satheesh, S.K.; Moorthy, K.K. Aerosol radiative forcing due to enhanced black carbon at an urban site in India. *Geophys. Res. Lett.* **2002**, *29*, 1880. [CrossRef]

28. Ramanathan, V.; Chung, C.; Kim, D.; Bettge, T.; Buja, L.; Kiehl, J.T.; Washington, W.M.; Fu, Q.; Sikka, D.R.; Wild, M. Atmospheric brown clouds: Impacts on South Asian Climate and hydrological cycle. *Proc. Natl. Acad. Sci.* **2005**, *102*, 5326–5333. [CrossRef] [PubMed]
29. Chung, C.E.; Ramanathan, V. Weakening of North Indian SST Gradients and the Monsoon Rainfall in India and the Sahel. *J. Clim.* **2006**, *19*, 2036–2045. [CrossRef]
30. Lau, K.M.; Kim, M.K.; Kim, K.M. Aerosol induced anomalies in the Asian summer monsoon: The role of the Tibetan Plateau. *Clim. Dyn.* **2006**, *26*, 855–864. [CrossRef]
31. Lau, K.; Ramanathan, V.; Wu, G.; Li, Z.; Tsay, S.C.; Hsu, C.; Sikka, R.; Holben, B.; Lu, D.; Tartari, G.; et al. The Joint Aerosol–Monsoon Experiment: A New Challenge for Monsoon Climate Research. *Bull. Am. Meteorol. Soc.* **2008**, *89*, 369–384. [CrossRef]
32. Lau, W.K.M.; Kim, M.K.; Kim, K.M.; Lee, W.S. Enhanced surface warming and accelerated snowmelt in the Himalayas and Tibetan Plateau induced by absorbing aerosols. *Environ. Res. Lett.* **2010**, *5*, 025204. [CrossRef]
33. Lau, W.K.M.; Kim, K.M. Competing influences of greenhouse warming and aerosols on Asian summer monsoon circulation and rainfall. *Asian Pac. J. Atmos. Sci.* **2017**, *53*, 181–194. [CrossRef]
34. Lau, W.K.M.; Kim, K.M.; Leung, L.R. Changing circulation structure and rainfall characteristics of the Asian monsoon: Greenhouse warming vs. aerosols. *Geosci. Lett.* **2017**, *4*, 28. [CrossRef]
35. Randles, C.A.; Ramaswamy, V. Absorbing aerosols over Asia: A Geophysical Fluid Dynamics Laboratory general circulation model sensitivity study of model response to aerosol optical depth and aerosol absorption. *J. Geophys. Res.* **2008**, *113*, D21203. [CrossRef]
36. Gautam, R.; Hsu, N.C.; Lau, K.M.; Tsay, S.C.; Kafatos, M. Enhanced pre-monsoon warming over the Himalayan-Gangetic region from 1979 to 2007. *Geophys. Res. Lett.* **2009**, *36*, L07704. [CrossRef]
37. Wang, C.; Kim, D.; Ekman, A.M.L.; Barth, M.C.; Rasch, P.J. Impact of anthropogenic aerosols on Indian summer monsoon. *Geophys. Res. Lett.* **2009**, *36*, L21704. [CrossRef]
38. Bollasina, M.; Ming, Y.; Ramaswamy, V. Anthropogenic aerosols and the weakening of the South Asian Monsoon. *Science* **2011**, *334*, 502–505. [CrossRef] [PubMed]
39. Ganguly, D.; Rasch, P.J.; Wang, H.; Yoon, J.-H. Climate response of the South Asian monsoon system to anthropogenic aerosols. *J. Geophys. Res.* **2012**, *117*, D13209. [CrossRef]
40. Lau, W.K.M. The Aerosol-Monsoon Climate System of Asia: A New Paradigm. *J. Meteorol. Res.* **2016**, *30*, 1–11. [CrossRef]
41. Li, Z.; Lau, W.K.M.; Ramanathan, V.; Wu, G.; Ding, Y.; Manoj, M.G.; Qian, Y.; Li, J.; Zhou, T.; Fan, J.; et al. Aerosol and Monsoon Climate Interactions over Asia. *Rev. Geophys.* **2016**, *54*, 866–929. [CrossRef]
42. Lau, K.M.; Kim, K.M. Observational relationships between aerosol and Asian monsoon rainfall, and circulation. *Geophys. Res. Lett.* **2006**, *33*, L21810. [CrossRef]
43. Lau, W.K.M.; Kim, K.M. Fingerprinting the impacts of aerosols on long-term trends of the Indian summer monsoon regional rainfall. *Geophys. Res. Lett.* **2010**, *37*, L16705. [CrossRef]
44. Meehl, G.A.; Arblaster, J.M.; Collins, W.D. Effects of Black Carbon Aerosols on the Indian Monsoon. *J. Clim.* **2008**, *21*, 2869–2882. [CrossRef]
45. D'Errico, M.; Cagnazzo, C.; Gogli, P.G.; Lau, W.K.M.; Hardenberg, J.; Fierli, F.; Cherchi, A. Indian monsoon and the elevated heat pump mechanism in a coupled aerosol-climate model. *J. Geophys. Res.* **2015**, *120*, 8712–8723. [CrossRef]
46. Kim, M.K.; Lau, W.K.M.; Kim, K.-M.; Sang, J.; Kim, Y.-H.; Lee, W.-S. Amplification of ENSO effects on Indian summer monsoon by absorbing aerosols. *Clim. Dyn.* **2016**, *46*, 2657–2671. [CrossRef]
47. Hazra, A.; Goswami, B.N.; Chen, J.-P. Role of interactions between aerosol radiative effect, dynamics, and cloud microphysics on transitions of monsoon intraseasonal oscillations. *J. Atmos. Sci.* **2013**, *70*, 2073–2087. [CrossRef]
48. Vinoj, V.; Rasch, P.J.; Wang, H.; Yoon, J.; Ma, P.; Landu, K. Short-term modulation of Indian summer monsoon rainfall by West Asian dust. *Nat. Geosci.* **2014**, *7*, 308–313. [CrossRef]
49. Lau, W.K.M.; Kim, K.M.; Shi, J.J.; Matsui, T.; Chin, M.; Tan, Q.; Peters-Lidard, C.; Tao, W.K. Impacts of aerosol–monsoon interaction on rainfall and circulation over Northern India and the Himalaya Foothills. *Clim. Dym.* **2016**, *49*, 1945–1960. [CrossRef]
50. Lau, W.K.M. Impacts of aerosols on climate and weather in the Hindu-Kush Himalayas-Gangetic region. *Clim. Sci.* **2018**. [CrossRef]

51. Flanner, M.G.; Zender, C.S.; Randerson, J.T.; Rasch, P.J. Present-day climate forcing and response from black carbon in snow. *J. Geophys. Res.* **2017**, *112*, D11202. [CrossRef]
52. Flanner, M.G.; Zender, C.S.; Hess, P.G.; Mahowald, N.M.; Painter, T.H.; Ramanathan, V.; Rasch, P.J. Springtime warming and reduced snow cover from carbonaceous particles. *Atmos. Chem. Phys.* **2009**, *9*, 2481–2497. [CrossRef]
53. Lee, W.-S.; Bhawar, R.L.; Kim, M.K.; Sang, J. Study of aerosol effect on accelerating snowmelt over the Tibetan Plateau during boreal spring. *Atmos. Environ.* **2013**, 113–122. [CrossRef]
54. Qian, Y.; Flanner, M.G.; Leung, L.R.; Wang, W. Sensitivity studies on the impacts of Tibetan Plateau snowpack pollution on the Asian hydrological cycle and monsoon climate. *Atmos. Chem. Phys.* **2011**, *11*, 1929–1948. [CrossRef]
55. Qian, Y.; Yasunari, T.J.; Doherty, S.J.; Flanner, M.G.; Lau, W.K.M.; Ming, J.; Wang, H.; Wang, M.; Warren, S.G.; Zhang, R. Light-absorbing Particles in Snow and Ice: Measurement and Modeling of Climatic and Hydrological impact. *Adv. Atmos. Sci.* **2015**, *32*, 64–91. [CrossRef]
56. Yasunari, T.J.; Koster, R.D.; Lau, W.K.M.; Kim, K.-M. Impact of snow darkening via dust, black carbon, and organic carbon on boreal spring climate in the Earth system. *J. Geophys. Res. Atmos.* **2015**, *120*, 5485–5503. [CrossRef]
57. Lau, W.K.M.; Sang, J.; Kim, M.K.; Kim, K.M.; Koster, R.D.; Yasunari, T.J. Impact of snow-darkening effects by light absorbing aerosols on hydro-climate of Eurasia, during boreal summer. *J. Geophys. Res.* **2018**, *123*. [CrossRef]
58. Xu, B.; Cao, J.; Hansen, J.; Yao, T.; Joswia, D.R.; Wang, N.; Wu, G.; Wang, M.; Zhao, H.; Yang, W.; et al. Black soot and the survival of Tibetan glaciers. *Proc. Natl. Acad. Sci. USA* **2009**, *106*, 22114–22118. [CrossRef] [PubMed]
59. Kopacz, M.; Mauzerall, D.L.; Wang, J.; Leibensperger, E.M.; Henze, D.K.; Singh, K. Origin and radiative forcing of black carbon transported to the Himalayas and Tibetan Plateau. *Atmos. Chem. Phys.* **2011**, *11*, 2837–2852. [CrossRef]
60. Rienecker, M.M.; Suarez, M.J.; Todling, R.; Bacmeister, J.; Takacs, L.; Liu, H.-C.; Gu, W.; Sienkiewicz, M.; Koster, R.D.; Gelaro, R.; et al. *The GEOS-5 Data Assimilation System—Documentation of Versions 5.0.1 and 5.1.0, and 5.2.0*; NASA Tech. Rep. Series on Global Modeling and Data Assimilation; NASA/TM-2008-104606; NASA Goddard Space Flight Center: Greenbelt, MD, USA, 2008; Volume 27, p. 92.
61. Ducharne, A.; Koster, R.D.; Suarez, M.J.; Stieglitz, M.; Kumar, P. A catchment-based approach to modeling land surface processes in a general circulation model: 2. Parameter estimation and model demonstration. *J. Geophys. Res.* **2000**, *105*, 823–824. [CrossRef]
62. Koster, R.D.; Suarez, M.J.; Ducharne, A.; Stieglitz, M.; Kumar, P. A catchment-based approach to modeling land surface processes in a general circulation model 1. Model structure. *J. Geophys. Res.* **2000**, *105*, 24809–24822. [CrossRef]
63. Lynch-Stieglitz, M. The development and validation of a simple snow model for the GISS GCM. *J. Clim.* **1994**, *7*, 1842–1855. [CrossRef]
64. Yasunari, T.J.; Tan, Q.; Lau, K.M.; Bonasoni, P.; Marinoni, A.; Laj, P.; Menegoz, M.; Takemura, T.; Chin, M. Estimated range of black carbon dry deposition and the related snow albedo reduction over Himalayan glaciers during dry pre-monsoon periods. *Atmos. Environ.* **2013**, *78*, 259–267. [CrossRef]
65. Yasunari, T.J.; Lau, K.M.; Mahanama, S.P.P.; Colarco, P.R.; da Silva, A.M.; Aoki, T.; Aoki, K.; Murao, N.; Yamagata, S.; Kodama, Y. The GOddard SnoW impurity module (GOSWIM) for the NASA GEOS-5 earth system model: Preliminary comparisons with observations in Sapporo, Japan. *SOLA* **2014**, *10*, 50–56. [CrossRef]
66. Chin, M.; Rood, R.B.; Lin, S.-J.; Müller, J.-F.; Thompson, A.M. Atmospheric sulfur cycle simulated in the global model GOCART: Model description and global properties. *J. Geophys. Res.* **2000**, *105*, 24671. [CrossRef]
67. Ginoux, P.; Chin, M.; Tegen, I.; Prospero, J.M.; Holben, B.; Dubovik, O.; Lin, S.-J. Sources and distributions of dust aerosols simulated with the GOCART model. *J. Geophys. Res.* **2001**, *106*, 20255–20273. [CrossRef]
68. Chin, M.; Ginoux, P.; Kinne, S.; Torres, O.; Holben, B.N.; Duncan, B.N.; Martin, R.V.; Logan, J.A.; Higurashi, A.; Nakajima, T. Tropospheric Aerosol Optical Thickness from the GOCART Model and Comparisons with Satellite and Sun Photometer Measurements. *J. Atmos. Sci.* **2002**, *59*, 461–483. [CrossRef]

69. Colarco, P.; da Silva, A.; Chin, M.; Diehl, T. Online simulations of global aerosol distributions in the NASA GEOS-4 model and comparisons to satellite and ground-based aerosol optical depth. *J. Geophys. Res. Atmos.* **2010**, *115*, D14207. [CrossRef]
70. Randles, C.A.; Colarco, P.R.; da Silva, A. Direct and semi-direct aerosol effects in the NASA GEOS-5 AGCM: Aerosol-climate interactions due to prognostic versus prescribed aerosols. *J. Geophys. Res. Atmos.* **2013**, *118*, 149–169. [CrossRef]
71. Reynolds, R.W.; Rayner, N.A.; Smith, T.M.; Stokes, D.C.; Wang, W. An improved in situ and satellite SST analysis for climate. *J. Clim.* **2002**, *15*, 1609–1625. [CrossRef]
72. Eck, T.F.; Holben, B.N.; Reid, J.S.; Dubovik, O.; Smirnov, A.; O'Neill, N.T.; Slutsker, I.; Kinne, S. Wavelength dependence of the optical depth of biomass burning, urban, and desert dust aerosols. *J. Geophys. Res.* **1999**, *104*, 31333–31349. [CrossRef]
73. Lau, K.M.; Kim, K.M.; Hsu, N.C.; Holben, B.N. Possible influences of air pollution, dust and sandstorms on the Indian monsoon. *WMO Bull.* **2009**, *58*, 22–30.
74. Pan, X.; Chin, M.; Gautam, R.; Bian, H.; Kim, D.; Colarco, P.R.; Diehl, T.L.; Takemura, T.; Pozzoli, L.; Tsigaridis, K.; et al. A multi-model evaluation of aerosols over South Asia: Common problems and possible causes. *Atmos. Chem. Phys.* **2015**, *15*, 5903–5928. [CrossRef]
75. Yanai, M.; Li, C.; Song, Z. Seasonal Heating of the Tibetan Plateau and Its Effects on the Evolution of the Asian Summer Monsoon. *J. Meteorol. Soc. Jpn. Ser. II* **1992**, *70*, 319–351. [CrossRef]
76. Wu, G.; Liu, Y.; Wang, T.; Wan, R.; Liu, X.; Li, W.; Wang, Z.; Zhang, Q.; Duan, A.; Liang, X. The Influence of Mechanical and Thermal Forcing by the Tibetan Plateau on Asian Climate. *J. Hydrometeorol.* **2007**, *8*, 770–789. [CrossRef]
77. Krishnamurti, T.N. Summer Monsoon Experiment—A Review. *Mon. Weather Rev.* **1985**, *113*, 1590–1626. [CrossRef]
78. Webster, P.J.; Yang, S. Monsoon and Enso: Selectively Interactive Systems. *Q. J. R. Meteorol. Soc.* **1992**, *118*, 877–926. [CrossRef]
79. Webster, P.J.; Magana, V.O.; Palmer, T.N.; Shukla, J.; Tomas, R.A.; Yanai, M.; Yasunari, T. Monsoons: Processes, predictability and the prospects for prediction. *J. Geophys. Res. Oceans* **1998**, *103*, 14451–14510. [CrossRef]
80. Wang, B. *The Asian Monsoon*; Springer: Heidelberg, Germany, 2006; p. 787. ISBN 978-3-540-40610-5.
81. Leary, C.A.; Houze, R.A. Melting and Evaporation of Hydrometeors in Precipitation from the Anvil Clouds of Deep Tropical Convection. *J. Atmos. Sci.* **1979**, *36*, 669–679. [CrossRef]
82. Sud, Y.C.; Walker, G.K. A Rain Evaporation and Downdraft Parameterization to Complement a Cumulus Updraft Scheme and Its Evaluation Using GATE Data. *Mon. Weather Rev.* **1993**, *121*, 3019–3039. [CrossRef]
83. Bacmeister, J.T.; Suarez, M.J.; Robertson, F.R. Rain Re-evaporation, Boundary Layer–Convection Interactions, and Pacific Rainfall Patterns in an AGCM. *J. Atmos. Sci.* **2006**, *63*, 3383–3403. [CrossRef]
84. Lau, K.M.; Kim, K.M.; Yang, S. Dynamical and Boundary Forcing Characteristics of Regional Components of the Asian Summer Monsoon. *J. Clim.* **2000**, *13*, 2461–2482. [CrossRef]
85. Ding, Y.; Chan, J.C.L. The East Asian summer monsoon: An overview. *Meteorol. Atmos. Phys.* **2005**, *89*, 117–142.
86. Sampe, T.; Xie, S. Large-Scale Dynamics of the Meiyu-Baiu Rainband: Environmental Forcing by the Westerly Jet. *J. Clim.* **2010**, *23*, 113–134. [CrossRef]
87. Zhou, T.-J.; Yu, R.-C. Atmospheric water vapor transport associated with typical anomalous summer rainfall patterns in China. *J. Geophys. Res.* **2005**, *110*, D08104. [CrossRef]
88. Li, C.F.; Yanai, M. The onset and interannual variability of the Asian summer monsoon in relation to land-sea thermal contrast. *J. Clim.* **1996**, *9*, 358–375. [CrossRef]
89. Xavier, P.K.; Marzin, C.; Goswami, B.N. An objective definition of the Indian summer monsoon season and a new perspective on the ENSO-monsoon relationship. *Q. J. R. Meteorol. Soc.* **2007**, *133*, 749–764. [CrossRef]
90. Lau, W.K.M.; Cheng, Y.; Li, Z. Origin, maintenance and variability of the Asian Tropopause Aerosol Layer (ATAL): Roles of monsoon dynamics. *Sci. Rep.* **2018**, *8*, 3960. [CrossRef] [PubMed]
91. Roesch, A. Evaluation of surface albedo and snow cover in AR4 coupled climate models. *J. Geophys. Res.* **2006**, *111*, D15111. [CrossRef]
92. Levy, R.C.; Leptoukh, G.G.; Kahn, R.; Zubko, V.; Gopalan, A.; Remer, L.A. A Critical Look at Deriving Monthly Aerosol Optical Depth from Satellite Data. *IEEE Trans. Geosci. Remote Sens.* **2009**, *47*, 2942–2956. [CrossRef]

93. Levy, R.C.; Remer, L.A.; Kleidman, R.G.; Mattoo, S.; Ichoku, C.; Kahn, R.; Eck, T.F. Global evaluation of the Collection 5 MODIS dark-target aerosol products over land. *Atmos. Chem. Phys.* **2010**, *10*, 10399–10420. [CrossRef]
94. Frei, A.; Tedesco, M.; Lee, S.; Foster, J.; Hall, D.K.; Kelly, R.; Robinson, D.A. A review of global satellite-derived snow products. *Adv. Space Res.* **2012**, *50*, 1007–1029. [CrossRef]
95. Lau, W.K.M. Desert Dust and Monsoon Rainfall. *Nat. Geosci.* **2014**, *7*, 255–256. [CrossRef]